BASIC SCIENCE

Nanomedicine: Nanotechnology, Biology, and Medicine
12 (2016) 399–409

nanomedicine
Nanotechnology, Biology, and Medicine

ELSEVIER

Original Article

nanomedjournal.com

Deterministic transfection drives efficient nonviral reprogramming and uncovers reprogramming barriers

Daniel Gallego-Perez, PhD[a,d,f,1], Jose J. Otero, MD, PhD[b,c,f,*,1], Catherine Czeisler, PhD[b,f], Junyu Ma, PhD[a], Cristina Ortiz, BSc[b,f], Patrick Gygli, PhD[b,f], Fay Patsy Catacutan, BSc[b,f], Hamza Numan Gokozan, MD[b,f], Aaron Cowgill[b,f], Thomas Sherwood, PhD[c], Subhadip Ghatak, PhD[d,f], Veysi Malkoc, PhD[a], Xi Zhao, PhD[a], Wei-Ching Liao, PhD[a], Surya Gnyawali, PhD[d,f], Xinmei Wang, PhD[a], Andrew F. Adler, PhD[e,2], Kam Leong, PhD[e,3], Brian Wulff, PhD[b,f], Traci A. Wilgus, PhD[b,f], Candice Askwith, PhD[c], Savita Khanna, PhD[d,f], Cameron Rink, PhD[d,f], Chandan K. Sen, PhD[d,f,*], L. James Lee, PhD[a,f,*]

[a]*Department of Chemical and Biomolecular Engineering, College of Engineering, The Ohio State University, Columbus, OH*
[b]*Department of Pathology, College of Medicine, The Ohio State University, Columbus, OH*
[c]*Department of Neuroscience, College of Medicine, The Ohio State University, Columbus, OH*
[d]*Department of Surgery, College of Medicine, The Ohio State University, Columbus, OH*
[e]*Department of Biomedical Engineering, Duke University, Durham, NC*
[f]*Center for Regenerative Medicine and Cell-Based Therapies (CRMCBT), The Ohio State University, Columbus, OH*

Received 10 September 2015; accepted 24 November 2015

Abstract

Safety concerns and/or the stochastic nature of current transduction approaches have hampered nuclear reprogramming's clinical translation. We report a novel non-viral nanotechnology-based platform permitting deterministic large-scale transfection with single-cell resolution. The superior capabilities of our technology are demonstrated by modification of the well-established direct neuronal reprogramming paradigm using overexpression of the transcription factors *Brn2*, *Ascl1*, and *Myt1l* (BAM). Reprogramming efficiencies were comparable to viral methodologies (up to ~9-12%) without the constraints of capsid size and with the ability to control plasmid dosage, in addition to showing superior performance relative to existing non-viral methods. Furthermore, increased neuronal complexity could be tailored by varying BAM ratio and by including additional proneural genes to the BAM cocktail. Furthermore, high-throughput NEP allowed easy interrogation of the reprogramming process. We discovered that BAM-mediated reprogramming is regulated by *AsclI* dosage, the S-phase cyclin *CCNA2*, and that some induced neurons passed through a nestin-positive cell stage.

From the Clinical Editor: In the field of regenerative medicine, the ability to direct cell fate by nuclear reprogramming is an important facet in terms of clinical application. In this article, the authors described their novel technique of cell reprogramming through overexpression of the transcription factors Brn2, Ascl1, and Myt1l (BAM) by in situ electroporation through nanochannels. This new technique could provide a platform for further future designs.

Key words: Induced neuron; Nuclear reprogramming; Transfection; Nanochannel electroporation

Competing financial interests: The authors declare no competing financial interests.

Funding was provided by NIBIB (1R21EB017539-01A1 and 3R21EB017539-01A1S1), National Science Foundation (NSEC EEC-0914790), National Center for the Advancing Translational Sciences (UL1TR001070 and 8UL1TR000090-05), NINDS P30 core grant (NS045758) and NIH GM069589, GM077185, GM108014, NS42617 and NR 013898. The content is solely the responsibility of the authors and does not necessarily represent the official views of the National Center for Advancing Translational Sciences, National Science Foundation or the National Institutes of Health. This work was sponsored by and represents activity of The Ohio State University Nanoscale Engineering Center for Affordable Nanoengineering of Polymeric Biomedical Devices and Center for Regenerative Medicine and Cell Based Therapies (regenerativemedicine.osu.edu).

* Corresponding authors at: Columbus, OH 43210.
E-mail addresses: jose.otero@osumc.edu (J.J. Otero), sen.16@osu.edu (C.K. Sen), lee.31@osu.edu (L.J. Lee).
[1] Equal contribution.
[2] Current address: Department of Neurosciences, University of California–San Diego, La Jolla, CA, USA, 92093.
[3] Current address: Department of Biomedical Engineering, Columbia University, New York, NY.

http://dx.doi.org/10.1016/j.nano.2015.11.015
1549-9634/

Directly inducing a specific cell fate requires not only the knowledge of which factors can stably induce a desired cell type, but also the ability to introduce these exogenous genes/proteins into cells in a controlled fashion. As has been elegantly demonstrated, nuclear reprogramming methodologies typically require relatively small cocktails of transcription factors to change a cell's epigenetic framework. For example, exogenous expression of *OCT4*, *KLF4*, *SOX2*, and *cMYC* reprograms fibroblasts into induced pluripotent stem (iPS) cells.[1] In addition, direct nuclear reprogramming of fibroblasts into post-mitotic neurons has been demonstrated by the forced expression of *Ascl1*, *Brn2*, and *Myt1l*.[2] These technologies provide significant opportunities to improve human health by advancing our understandings of basic cell biology, by facilitating the modeling of human diseases for pre-clinical drug development pipelines, and, ultimately, for clinically-relevant cell therapies.

For regenerative medicine and disease modeling applications, it may be more desirable to induce cells directly to the lineage of interest rather than by first proceeding through an iPS cell stage. This represents a unique challenge in cases where the cell of interest is post-mitotic and underscores the need to discover deterministic transfection methodologies for reprogramming applications. For example, to obtain a high quantity of neurons from direct neuronal reprogramming of dermal fibroblasts, a large number of cells would have to undergo the reprogramming process deterministically. Such reprogramming strategies would require the ability to control the transdifferentiation of large numbers of cells. Although significant advances have been made in reprogramming paradigms, including the implementation of small molecules and pharmaceutical approaches,[3-7] the ability to directly control the dosage of reprogramming factors in each individual cell has not yet been achieved. Furthermore, the stochastic barriers to implementing this long term vision have not been identified.

The most widely implemented non-viral transfection approaches depend upon diffusion- and endocytosis-based mechanisms, resulting in stochastic transfections.[8] We have overcome this problem by developing a novel and easy-to-use device that permits *in situ* electroporation on cultured cells through a 3D ordered array of nanochannels. Such an array was created via the adaptation of conventional Transwell inserts, which are commonly used in routine cell culture, for nanochannel electroporation (NEP). NEP is a single-cell transfection system that electrophoretically delivers charged agents directly into the cytosol by applying an intense electric field over a small area of the cell membrane,[9] thus facilitating precise dosage control with minimum cell damage. A significant advantage of NEP over other electroporation paradigms is the benign nature of the transfection, resulting in negligible perturbations to cell physiology.[9] Although other electroporation modalities have similarly demonstrated enhanced transfection control of various types of engineered molecules with minimal cell toxicity,[10,11] deterministic transfection technologies for nuclear reprogramming applications have remained elusive. We validated the superiority of our novel NEP platform with a well-established direct nuclear reprogramming model that involves fibroblast transdifferentiation into neurons by exogenous expression of *Brn2*, *AscII*, and *Myt1l* (BAM). We found that the NEP platform was superior to bulk electroporation (BEP) with regard to reprogramming efficiency, showing iN generation at levels comparable to reports using lentivirus. Moreover, due to the inherent deterministic advantages of the NEP methodology, we were also able to demonstrate that nuclear reprogramming by BAM is regulated by *AscII* dosage, is regulated by the S-phase cyclin *CCNA2*, can be enhanced by adding proneural genes to the NEP cocktail, and that at least some neurons induced through BAM-mediated neuronal reprogramming may pass through a nestin-positive cell stage.

Methods

NEP platform fabrication

Unmodified Transwell inserts possess a highly dense and random array of nanochannels whose interactions with plated cells cannot be controlled at the single cell level. This could potentially result in high intercellular variability in the transfection characteristics among other things. Using standard cleanroom technologies (Figure 1, Figure S1), the apical or basal surface of the Transwells was spin coated (CE 100CB Resist Coater) with positive photoresist (S1813 or SPR-220.7) at ~3000 rpm for 1 min. The devices were subsequently soft-baked at room temperature for >16 h. The resist was then controllably exposed to UV light through a dark field photomask with circular openings of varying diameters using a contact aligner (EV Group 620 Advanced Contact Aligner). Following exposure, the photoresist was developed in positive resist developer for 1-2 min, which exposed the underlying nanopores on the Transwell membrane in an arrayed and orderly manner. Further details of the fabrication procedure are presented in the Supplementary materials.

Cell culture and transfections

BEP-based transfection

A Neon (Life Technologies) transfection system was used for BEP transfection. The cells were resuspended at a final concentration of 1.0×10^6 cells, in 0.1 ml. The cell suspension was then mixed with the plasmid solution (final plasmid concentration = 0.05-0.1μg/μl), and the tip was then inserted into the Neon tube containing the electrolytic buffer. The cells were electroporated following a protocol suggested by the manufacturer (one 30 ms pulse of 1350 V) optimized for MEF cells. BEP-based transfection outside these conditions could result in reduced efficacy and/or increased MEF cell death.

NEP-based transfection

MEF cells were directly loaded on the entire apical surface of the Transwell membrane at a density of ~$1.0\text{-}1.5 \times 10^4$ cells/cm^2 in regular maintenance medium (Figure 1, *A*). The cells were allowed to adhere and spread overnight before NEP transfection. Alternatively, cells could be selectively plated directly on top of the exposed nanochannels on the apical surface of the Transwell by controllably applying dielectrophoretic forces across the Transwell (Figure S1). Following cell loading, the media in the apical chamber were replaced by PBS and the Transwell inserts were then mounted on an e-beam evaporated

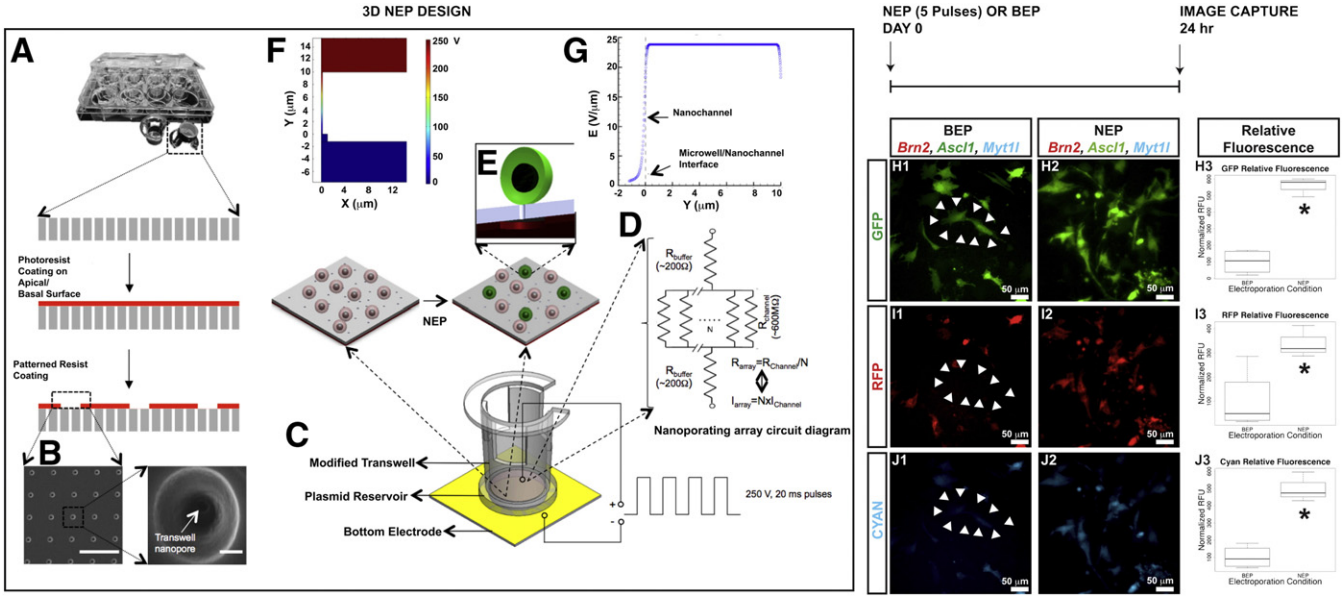

Figure 1. 3D NEP design delivers high dose plasmid DNA at single cell resolution with lower biological variability.**(A)** Photolithography-based adaptation of Transwell insert into a 3D NEP platform.**(B)** SEM of the modified insert surface showing a patterned microwell array (left, scale bar = 50 µm) over the nanochanneled membrane. Only exposed nanochannels (right, scale bar = 1 µm) can NEP-transfect the cells loaded on the apical side of the membrane.**(C)** Schematic diagram of how the transfection is conducted using the modified Transwell inserts.**(D)** Circuit diagram for the in-parallel array of nanochannels illustrating the relationship between the resistance across the membrane and the number of actively nanoporating channels.**(E)** Schematic illustration of a cell sitting directly on top of a nanoporating channel.**(F, G)** Finite element modeling of the electric field distribution during nanoporation. The electric field is maximized within the nanochannel which leads to enhanced and highly localized transmembrane potentials on the cells.**(H-J)** Bicistronic constructs for *Ascl1*, *Brn2*, and *Myt1l* (color coded green, red, and blue) were introduced into MEFs by NEP. Cells were allowed to recover for 24 h as indicated on the schematic, and epifluorescent photomicrographs were captured. NEP cells are compared to cells that underwent BEP in parallel experiments. Arrowheads demarcate the same cell in the different panels. Mean fluorescent intensity was obtained from ImageJ and plotted in the respective channels. In addition to showing a higher cellular mean fluorescent intensity, the nanochannel electroporated cells showed a much smaller interquartile range in fluorescent intensities, indicating a more uniform delivery across cells that underwent the NEP. Asterisk indicates statistical significance ($P < 0.05$ by *T*-test). Box plot shows a solid line at the mean, the height of the box is the interquartile range, and the maximum length of whiskers is 1.5 times the interquartile range. Panels H1 and H2 represent GFP fluorescence as a proxy for *Ascl1* transcript expression for BEP, and NEP, and the normalized fluorescence is box-plotted in H3. Panels I1 and I2 represent RFP fluorescence as a proxy for *Brn2* transcript expression for BEP, and NEP, and the normalized fluorescence is box-plotted in I3. Panels J1 and J2 represent CFP fluorescence as a proxy for *Mytl1* transcript expression for BEP, and NEP, and the normalized fluorescence is box-plotted in J3.

(Denton DV-502A E-Gun Evaporator) gold electrode that was in direct contact with the plasmid solution (Figure 1, *C*). A counter-electrode was then immersed in the PBS of the apical chamber, and a square wave pulse (250 V, 20 ms duration pulse, 1-10 pulses) was applied across the electrodes using a Biorad Gene Pulser Xcell power supply. The PBS was replaced by fresh media immediately after, and the cells were then incubated overnight at 37 °C.

Induced neuron protocol

Post-NEP, MEFs were cultured in N3 media. N3 neuronal induction medium was prepared by supplementing DMEM/F-12 (Invitrogen) base media with 25 µg/ml bovine insulin, 30 nmol/l sodium selenite, 50 µg/ml human apo-transferrin, 20 nmol/l progesterone, 10 ng/ml human bFGF2, and 100 µmol/l putrescine.

Statistical analysis

All statistics were performed in Rv2.12, Microsoft Excel, and Matlab. Sholl analysis and dendrite complexity index were performed using Neurolucida Explorer™ v11.

Results

An easy-to-use platform for deterministic large scale cell transfection

Figure 1, *A* illustrates the device design. Briefly, an array of nano- to micro-scale wells were patterned on the nanochanneled Transwell membrane surface to (*i*) minimize cytotoxic currents during electrotransfection, and (*ii*) to better control the extent of interaction of single cells with the nanoporating channels (Figure S1, *A*). This in turn leads to controlled dosage at the single cell level. The cells are then loaded on the apical surface, which is subsequently mounted within a pair of electrodes over a reservoir containing the cargo solution (Figure 1, *C*). A square wave DC pulse with a 250 V amplitude and a 20 ms pulse duration is then applied across the electrodes to porate the cells (Figure 1, *D-G*) directly delivering cargo into the cytosol.

This 3D NEP platform was validated by transfecting three cDNA expression constructs at a 1:1:1 molar ratio as model cargo into mouse embryonic fibroblasts (MEFs). We utilized reprogramming constructs designed with bicistronic fluorescent reporters; signals in cyan (*Myt1l*), red (*Brn2*), and green (*Ascl1*) indicated successful transcription of BAM mRNA. Bulk electroporation (BEP)[12] was used as a control transfection method. Although BAM transfection by NEP or BEP resulted in

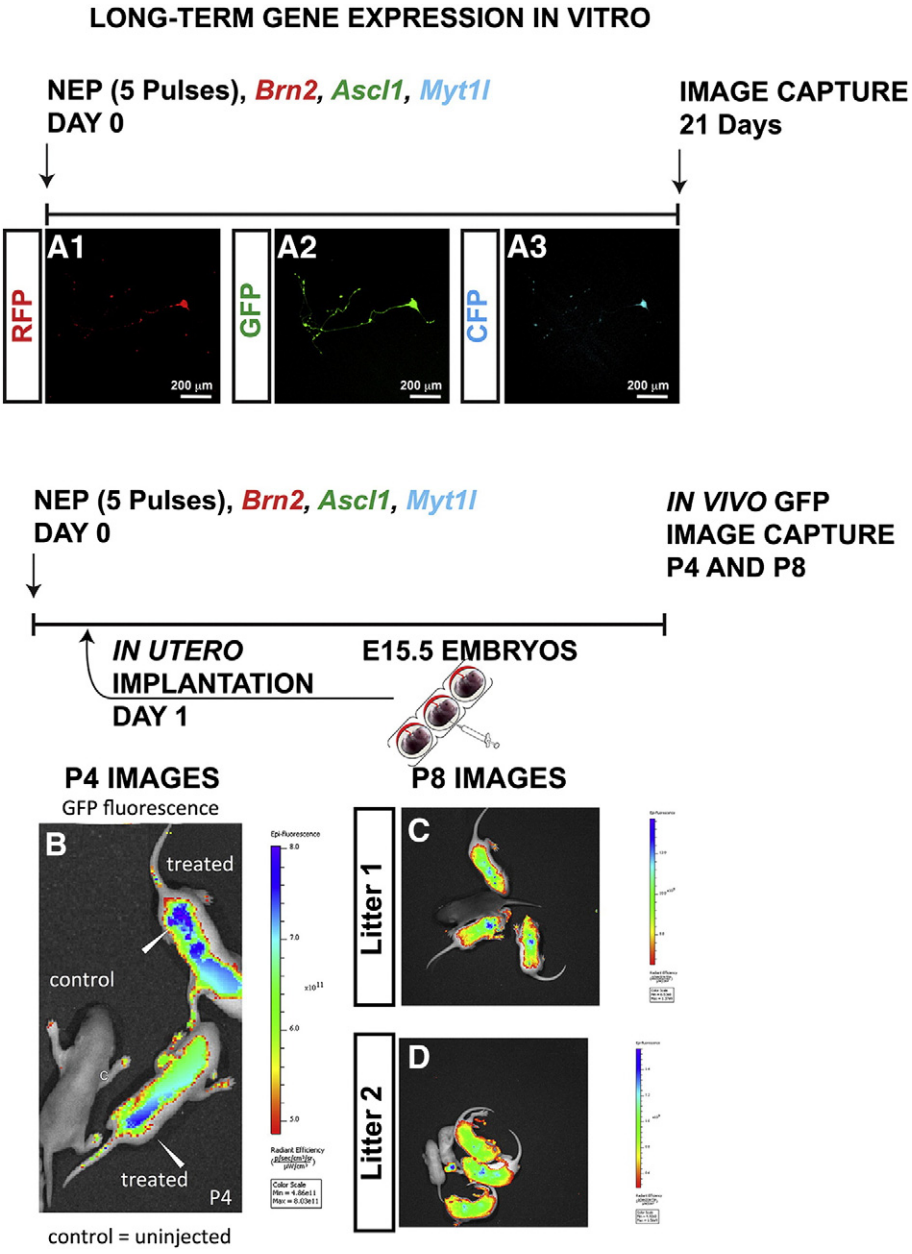

Figure 2. Persistent long-term expression of BAM reporter constructs *in vitro* and *in vivo*.**(A)** MEFs were transfected with BAM cDNA expression plasmids designed to have a bicistronic transcript for fluorescent tagging as follows: *Ascl1::GFP*, *Brn2::RFP*, *Myt1l::CFP*. Cells were differentiated for 21 days. Endogenous fluorescence was captured in an epifluorescence microscope and demonstrates continued expression of the plasmids at 21 days. On day 1 post-NEP, cells were implanted *in utero* to E15.5 embryos. Pups were analyzed by *in vivo* imaging on post-natal days 4 and 8 for GFP expression.**(B)** Animals were imaged on post-natal day 4 (**C-D**, each photograph represents a different litter).

relatively early (~4 h) *Ascl1* plasmid expression, NEP-based transfection led to significantly higher and more uniform transfection extent compared to BEP (Figure S1, *P*). Moreover, NEP conditions could be easily tailored to control the dosage (Figure S1, *P3*). We compared NEP-treated cells with the upper 2% BEP-transfected cells (as sorted by FACS of GFP-positive cells) and found that even though the mean RFU of this BEP subset was similar to that of the NEP 5-pulse group, the NEP-treated cells had improved viability and a smaller interquartile range in RFU relative to the BEP cells (Figure S1, *Q*). The top 2% BEP cells were viable for less than 2 days.

Co-expression of all three plasmids was detected 24 h after transfection. When comparing GFP/RFP/CFP-positive cells, NEP 5-pulse resulted in significantly higher mean relative fluorescence expression compared to BEP (Figure 1, *H-J*). Moreover, the fluorescence intensity variance among NEP-treated cells was significantly lower compared to BEP. In addition, while all the clones in the NEP group had a tendency to successfully co-express all three plasmids, a host of cells in the BEP group only showed detectable expression of one or two of the three plasmids (Figure 1, *H1-J1* arrowheads). Persistent long-term expression of BAM reporter constructs was seen in a number of cells in the NEP group (Figure 2).

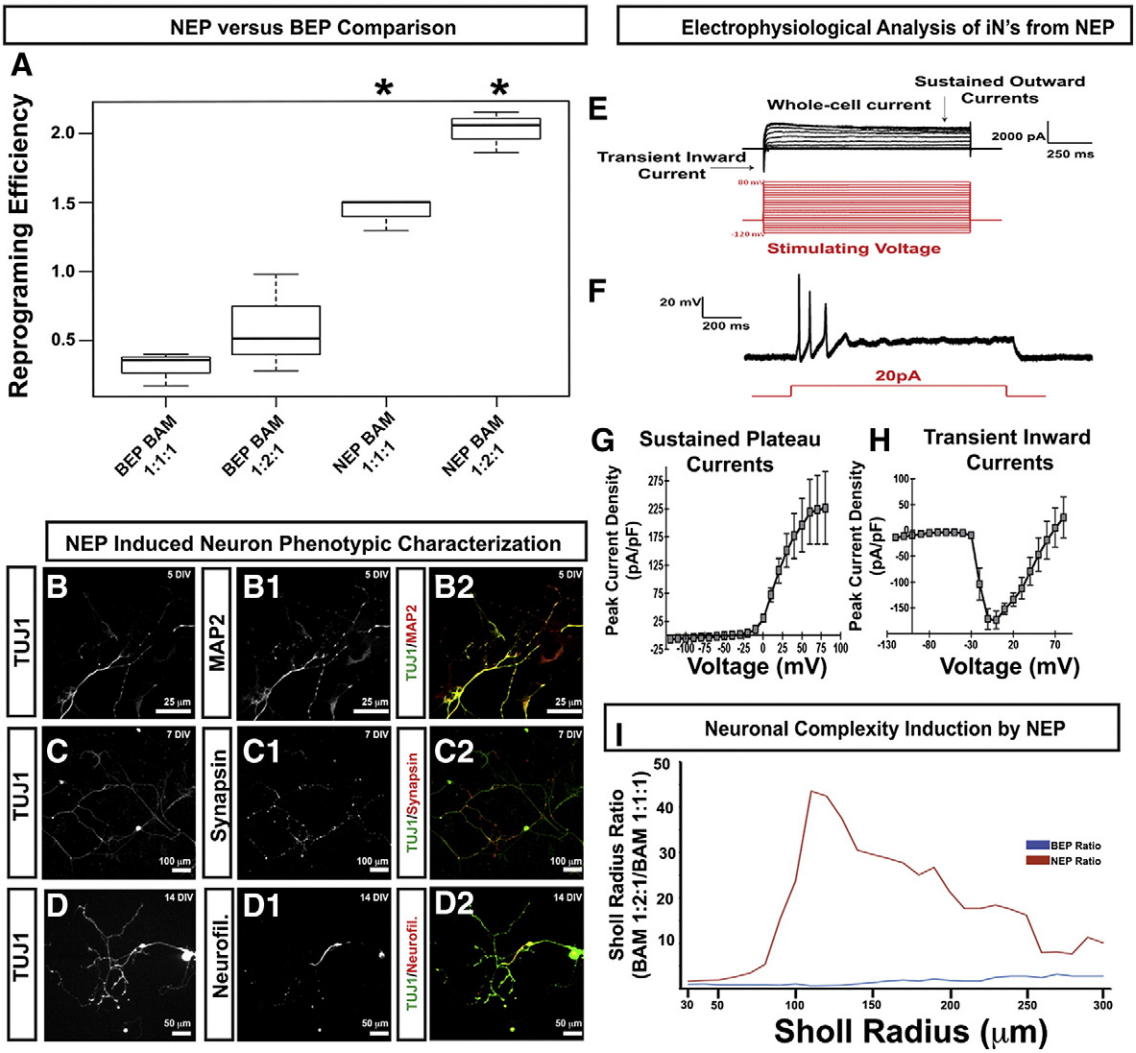

Figure 3. Induced Neuron Formation by NEP.**(A)** TUJ1 quantification of stained cells 7 days post-BEP or post-NEP using either equimolar ratios of plasmid DNA or molar ratios of 1:2:1 of *Brn2*, *Ascl1*, and *Myt1l*, respectively. Neuronal reprogramming efficiency (defined as 100 × total neuron number/seeding density) is plotted as a function of electroporation condition. Asterisks indicate statistical significance from the three other groups ($P < 0.05$).**(B-D)** Phenotypic characterization of induced neurons post-NEP at 14 days. Molecular markers are indicated on the left of each panel.**(E)** Electrophysiology of neurons 20-days post-NEP. Cells display the necessary voltage-gated currents to fire action potentials. Both transient inward currents and sustained outward currents were observed in response to depolarizing voltage simulations.**(F)** A typical response to a 20 pA current injection is illustrated and indicates that cells fired action potentials in response to depolarizing current.**(G-H)** Voltage–current relationship quantification for the transient and sustained components of whole-cell current. Sustained plateau currents are shown in G, and transient inward currents are shown in H.**(I)** Neuronal complexity index of induced neurons by Sholl analysis. The y-axis is the ratio of mean number of intersections between BAM at 1:2:1/1:1:1, x-axis is distance from neuron cell body. Supplementary Table S4 shows inferential statistics.

This was further confirmed by *in vivo* studies in which MEFs underwent NEP of *BAM* prior to being subcutaneously injected into E15.5 embryos *in utero*. Postnatal day 4 pups that had undergone embryonic transplanation showed significant GFP expression by *in vivo* IVIS imaging (Figure 2) compared to control pups. We conclude that NEP-based transfection results in stronger and more uniform gene expression compared to BEP, and that such expression showed stable and long-lasting behavior both *in vitro* and *in vivo*.

Deterministic NEP-based delivery leads to efficient and controlled transfection

In order to further test the effects of a more deterministic transfection approach in reprogramming outcome, we cultured the transfected MEFs in N3 media for a prolonged period of time and monitored induced neuron (iN) formation by assaying neuronal marker expression, morphological changes, and electrophysiological activity. NEP-treated cultures showed significantly higher and more narrowly-distributed early (day 7) reprogramming efficiencies (based on number of TUJ1+ cells) across samples compared to BEP (Figure 3, *A*). Following transfection, a number of NEP-treated cells started to show significant morphological changes compatible with neuronal transformation within remarkably short timeframes (<48 h, Supplementary Video 1), exhibiting slightly faster kinetics compared to viral infection.[2] NEP of human dermal fibroblasts with BAM plasmids also showed rapid morphological changes suggestive of reprogramming (Figure S1, *R*). Mature neuronal

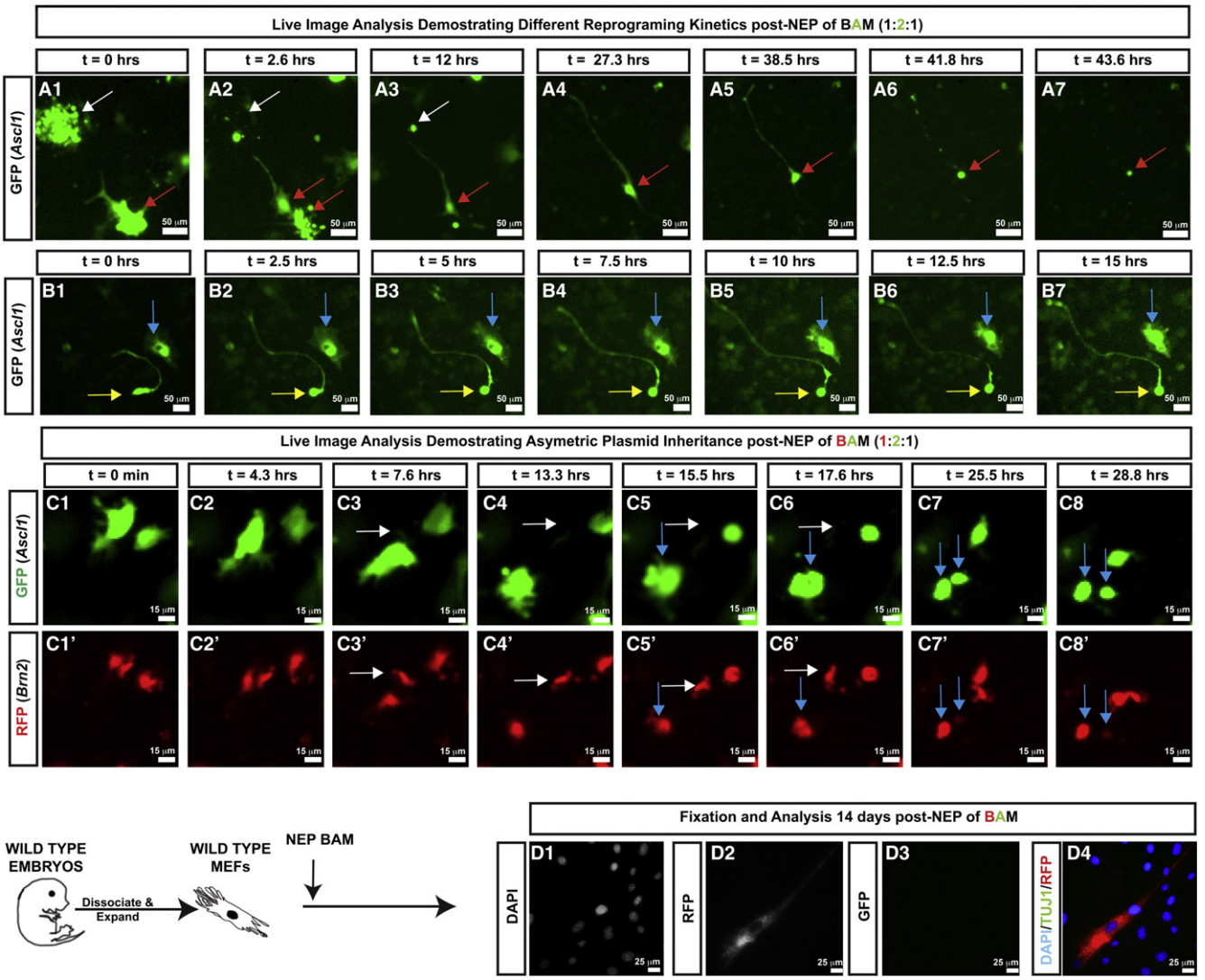

Figure 4. Stochastic barriers to neuronal reprogramming.**(A-B)** Time-lapse photography of neuronal reprogramming post-NEP. In these images, the time course is delineated in the box above the figure. White arrow in A-series denotes an *Ascl1*-IRES-*GFP*-positive cell undergoing degeneration. Red arrow in A-series denotes a cell that first undergoes cell division with one daughter cell undergoing degeneration, with the second cell showing robust reprogramming but then ultimately cellular degeneration. Blue arrow in B-series shows an *Ascl1*-IRES-*GFP*-positive cell without morphological evidence of reprogramming. Yellow arrow in B-series shows an *Ascl1*-IRES-*GFP*-positive cell with successful reprogramming that shows robust neurite growth.**(C-C')** White arrow denotes cell with silenced *Ascl1-GFP* but with preserved *Brn2-RFP*. Blue arrow denotes a cell division resulting in near-symmetric inheritance of *Ascl1-GFP* but asymmetric inheritance of *Brn2-RFP*. Molecular marker is on left, the time post-NEP is on the top of each panel. Images from cells in panels A and C were started 4-6 h after NEP of *BAM*. Cells in panel B were imaged 3 days after NEP.**(D)** Endogenous silencing of exogenous *Ascl1*-IRES-*GFP*. Note that *Ascl1*-silenced cells do not become TUJ1 positive.

marker (MAP2, synapsin and neurofilament) expression in the NEP group was similarly detected very early post-NEP (week 1). Moreover, NEP-treated cells also showed electrophysiological activity as demonstrated by their capacity to undergo induced action potentials (Figure 3, *E-H*).

A single NEP-based transfection was enough to reprogram a higher proportion of iNs in a shorter period of time compared to previous reports on non-viral iN reprogramming.[13] Nevertheless, a relatively large proportion of MEFs still had not shown signs of iN reprogramming at our experimental end-points. We hypothesized that this was partly due to the fact that *Ascl1* plasmid expression appears to be rapidly and selectively silenced in a number of MEF cells (Supplementary Video 2). *Brn2* and *Myt1l* expression on the other hand seemed to be less prone such silencing.

We therefore increased the dosage of *Ascl1* relative to *Brn2* and *Myt1l* in NEP so as to determine a more optimal dosage of *BAM* cDNA expression plasmids for neuronal reprogramming. The current status quo for controlling molar ratios of reprogramming genes is to deliver them in a multicistronic expression plasmid[12] or implement TEVP-mediated proteolytic cleavage.[14] We found that increasing the relative molar ratio of *Ascl1* to 2:1:1 (*Ascl1:Brn2:Myt1L*) resulted in a more sharply enhanced reprogramming efficiency in the NEP group compared

to BEP by day 7 post-transfection (Figure 3, *A*). Moreover, altering the molar ratio of BAM also led to increased neuronal morphological complexity in NEP treated cells (Figure 3, *I*). BEP-treated MEFs, instead, showed no clear change in morphology in response to the altered BAM ratio. We conclude that the NEP technology is a better-suited approach not only for enhanced but also for more controlled transfection and reprogramming. We also note that current technologies, including BEP and viral-based technologies, cannot achieve such tailorable reprogramming.

Prior studies have shown that specific neuronal traits could be induced by including additional proneural genes in the reprogramming cocktail.[15] Efficient multi-factor delivery, however, is extremely challenging with viral or non-viral transfection technologies. NEP on the other hand has the ability to deliver such complex combinations in a more deterministic manner at the single cell level. The unique control that NEP provides when transfecting multiple plasmids allows the rapid and well-controlled screening of many transcription factor combinations for desired phenotypes following direct reprogramming. As our model, we used information from the mammalian embryonic hindbrain development, which has a well-characterized gradient of dorsal-ventral and rostro-caudal patterning genes. We identified and selected additional proneural transcription factors, *PHOX2B*, *PHOX2A*, and *RUNX3* that are involved in patterning of autonomic hindbrain neurons.[16,17] Plasmids encoding for such factors, in combination with BAM, were then NEP-transfected into MEFs. Transfected cultures were then analyzed for marker expression and morphometry. Our results showed a slight increase in reprogramming efficiency by day 14 after transfection for the BAM/PHOX2B/PHOX2A/RUNX3 group relative to BAM only (mean iN reprogramming efficiency = 12% for BAM-PPR and 9% for BAM alone, Figure S2). As such, our approach achieved reprogramming efficiencies comparable to viral methodologies but without the constraints of capsid size, and with the ability to control plasmid dosage at the single cell level. We therefore analyzed neuronal maturity by morphometric analyses. Morphometric analyses of the iNs showed the most marked changes between groups, with iNs from the six-factor cocktail exhibiting more complex and mature neuronal morphologies compared to BAM alone. We conclude that NEP can improve the quality of neuronal reprogramming by increasing the morphological complexity of the neurons generated. Furthermore, since adding additional neuronal proneural genes resulted in only a modest, albeit significant, increase in neuronal reprogramming efficiency, we conclude that several barriers exist to the efficient generation of induced neurons that are not solved by more deterministic plasmid delivery.

NEP helps probe and uncover novel stochastic barriers to iN formation

Although NEP-based transfection ultimately resulted in relatively high reprogramming efficiencies, comparable to viral methodologies, a considerable proportion of MEFs appear to be less amenable to reprogramming. We thus designed experiments to determine cellular mechanistic barriers to direct neuronal reprogramming. Our time-lapse monitoring of BAM/NEP-treated MEFs is illustrated in Figure 4 and in videos 1-4 in the Supplementary Material. Instances of cells showing neuronal morphology could be identified as early as 15 h post-NEP (Figure 4, *A*). We note that some cells showed rapid and selective plasmid silencing (Supplementary Video 2 and Figure 4), and that some cells also underwent divisions coupled with asymmetric plasmid inheritance after a division (Figure 4). We thus proceeded to use NEP to further probe the stochastic aspects of iN reprogramming by focusing on the cell cycle, and the potential role of alternative intermediary pathways in the reprogramming process.

Regulatory factors upstream of Ascl1 discovered by NEP

Ascl1 pioneer activity is in part mediated by the interaction (direct or indirect) with the trivalent chromatin signature that includes H3K4me1, H3K27ac, and H3K9me3.[18] Therefore, although the *Ascl1* DNA consensus site clearly plays a key role, *Ascl1* pioneer activity would require additional factors capable of sensing certain chromatin states. We therefore utilized the NEP platform to explore the potential roles of the S-phase cyclin *CCNA2* in neuronal reprogramming. *CCNA2* has a well-established, albeit somewhat unappreciated role, in chromatin regulation. First, in S-phase, the chromatin landscape undergoes dramatic alterations as the entire genome is duplicated. *CCNA2*'s role as an initiator of replication origin[19] thus insinuates a role as a chromatin sensor. With this in mind, we isolated MEFs from pups harboring a homozygous targeted *CCNA2* allele that undergoes ablation after *cre*-mediated recombination. We used two methods to ablate the *CCNA2* locus. $CCNA2^{fl/fl}$ MEFs were either infected with an adenovirus-*cre* (or adenovirus-*Lacz* as a negative control) after BAM NEP resulting in *cre* expression several hours after *BAM* expression (Figure 5), or directly co-transfected with a pCag-*cre* plasmid resulting in simultaneous *cre* expression in the presence of BAM. The cells were kept in culture for 14 days and the extent of reprogramming was measured in terms of *β-tubulin III* expression (Figure 5, *A-D*). Although we found that the adenovirus-*cre*-infected cultures still showed clear signs of *β-tubulin III* expression, the cultures that were co-transfected with the pCag-*cre-GFP* plasmid concurrently with BAM during NEP clearly showed impaired reprogramming efficiency, with *cre*-positive $CCNA2^{fl/fl}$ cells often showing weak and very diffused TUJ1 staining patterns, and persistent fibroblast-like morphology after 14 days. Moreover, RT-PCR analysis showed clear downregulation of *β-tubulin III* gene expression in *cre*-positive cultures. The implications of this are two-fold: (1) direct cytosolic injection of plasmids by NEP facilitates rapid and more synchronous co-expression of the genes of interest (BAM + *cre*), thus presumably resulting in *CCNA2* ablation at the early stages of cell reprogramming; (2) the underlying methodology of viral transfection, on the other hand, promoted delayed *cre* gene expression relative to BAM likely due to both timing of infection in addition to gene delivery, resulting in subsequent late *CCNA2* ablation along the reprogramming pathway. Altogether these observations suggest that *CCNA2* could potentially be playing a more prominent role in the regulation of early events in BAM-mediated neuronal reprogramming, and that beyond a certain point along the reprogramming trajectory, *CCNA2* deletion does not appear to have a marked effect on the reprogramming outcome. This dependency on *CCNA2* activity

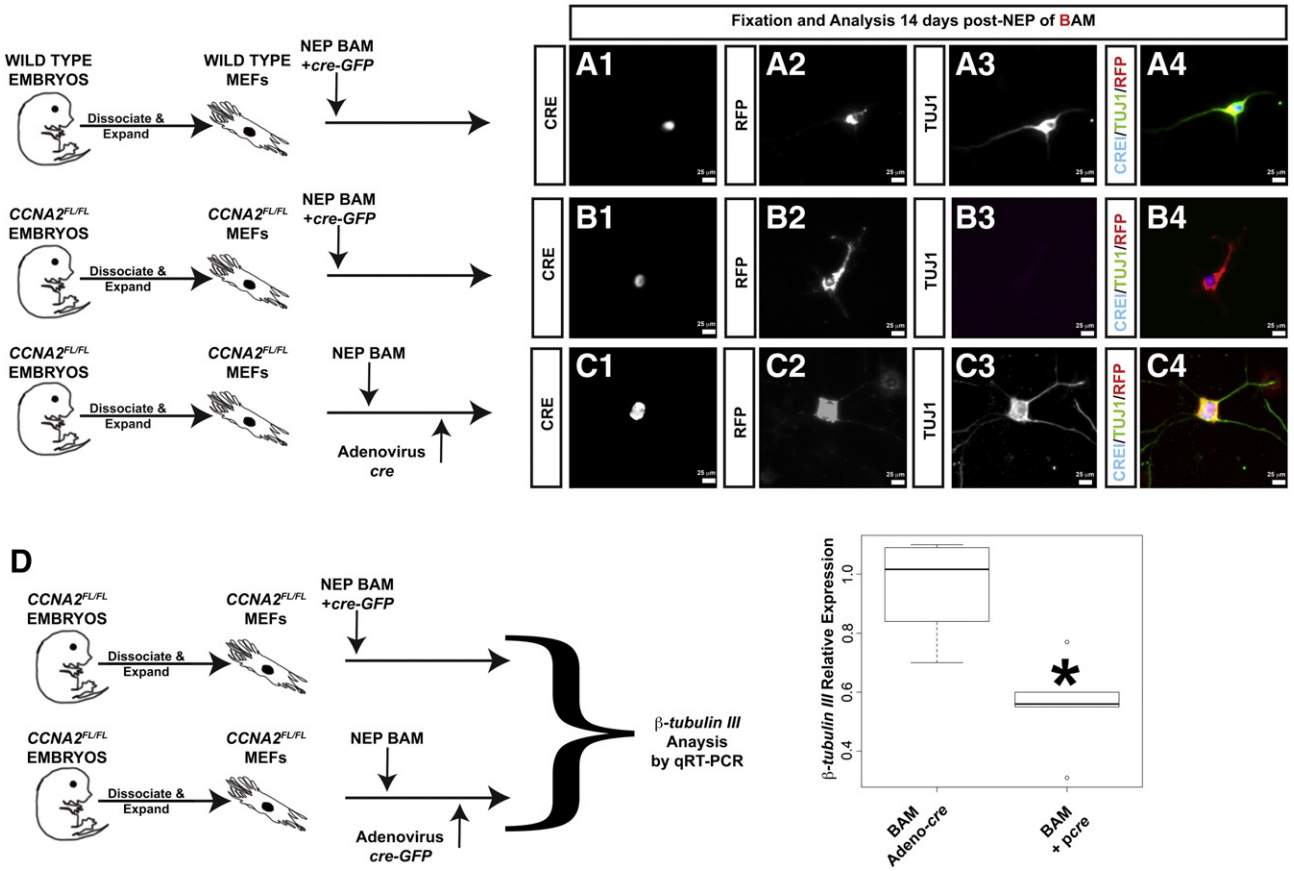

Figure 5. *CCNA2* ablation decreases neuronal reprogramming efficiency.**(A-C)** Targeted ablation of *CCNA2* early hinders neuronal reprogramming. Experimental schematics are illustrated to the left of each panel. Molecular markers are denoted on the left of each panel. Images represent epifluorescent photomicrographs. Panels A1-A4 represent images obtained from reprogramming of wild-type MEFs with *BAM* plus *cre-GFP* 14 days post-NEP. Panels B1-B4 represent images obtained 14 days post-NEP from MEFs obtained from CCNA2fl/fl embryos transfected with *BAM* plus *cre-GFP*. Panels C1-C4 represent images obtained from CCNA2fl/fl MEFs transfected first with BAM, and then infected with adenovirus-*cre-GFP* 6 h post-NEP.**(D)** *β-tubulin III* Qrt-PCR demonstrates significant decrease in *pCre* conditions relative to Adeno-*cre* conditions.

raises the point that cells may have to be in the appropriate cell cycle phase when receiving exogenous reprogramming factors to successfully undergo iN induction.

NEP discovers alternative intermediary pathways in the reprogramming process

Our findings of an S-phase cyclin as a potential pathway component of BAM-mediated reprogramming raise the possibility that at least a subset of reprogramming cells undergo S-phase. As this is improbable for mature neurons, we postulated that during the transition some somatic cells may first revert to a neural progenitor phase, followed by cell amplification and/or differentiation. A limited number of studies with conflicting results have looked into the potential role intermediate progenitor-like stages (i.e., neural progenitor cells) could play in BAM-mediated iN reprogramming.[20] To further probe this, we evaluated mRNA expression of the neural stem cell marker *nestin* in MEFs 24 h after NEP-based delivery of BAM. We found that dose-controlled delivery of BAM by NEP showed a significant increase in *nestin* expression, which positively correlated with exogenous *Ascl1* delivery/expression (Figure 6, *B*). In addition, immunostaining results 14 days after NEP-based delivery of BAM showed a number of nestin-positive cells that were still actively expressing exogenous *Ascl1/GFP* (Figure 6, *A*).

In order to further determine if a subset of the neurons resulting from NEP/BAM-mediated reprogramming underwent a transient nestin positive cell phase, we generated MEFs carrying the following two loci: *Nestin-cre-ER*, and *Rosa*$^{mTdTomato/mGFP}$. These MEFs express membrane-bound TdTomato in the absence of *cre*, whereas cells expressing a membrane-bound GFP indicate that *cre*-mediated excision occurred at some point in their ancestry. MEFs were treated with 1 μM 4-OH to stimulate the *CRE-ER* construct and cells underwent BAM-mediated reprogramming by NEP. In this case we used BAM plasmids that did not carry a fluorescent reporter gene. 4-OH was maintained in the culture media throughout the reprogramming process. Cells at 1, 7 and 14 days were fixed in 4% paraformaldehyde, and neuronal reprogramming of GFP-positive cells was determined. These conditions showed a significant increase in the number of GFP-positive cells (Figure 6, *C-E*). We found

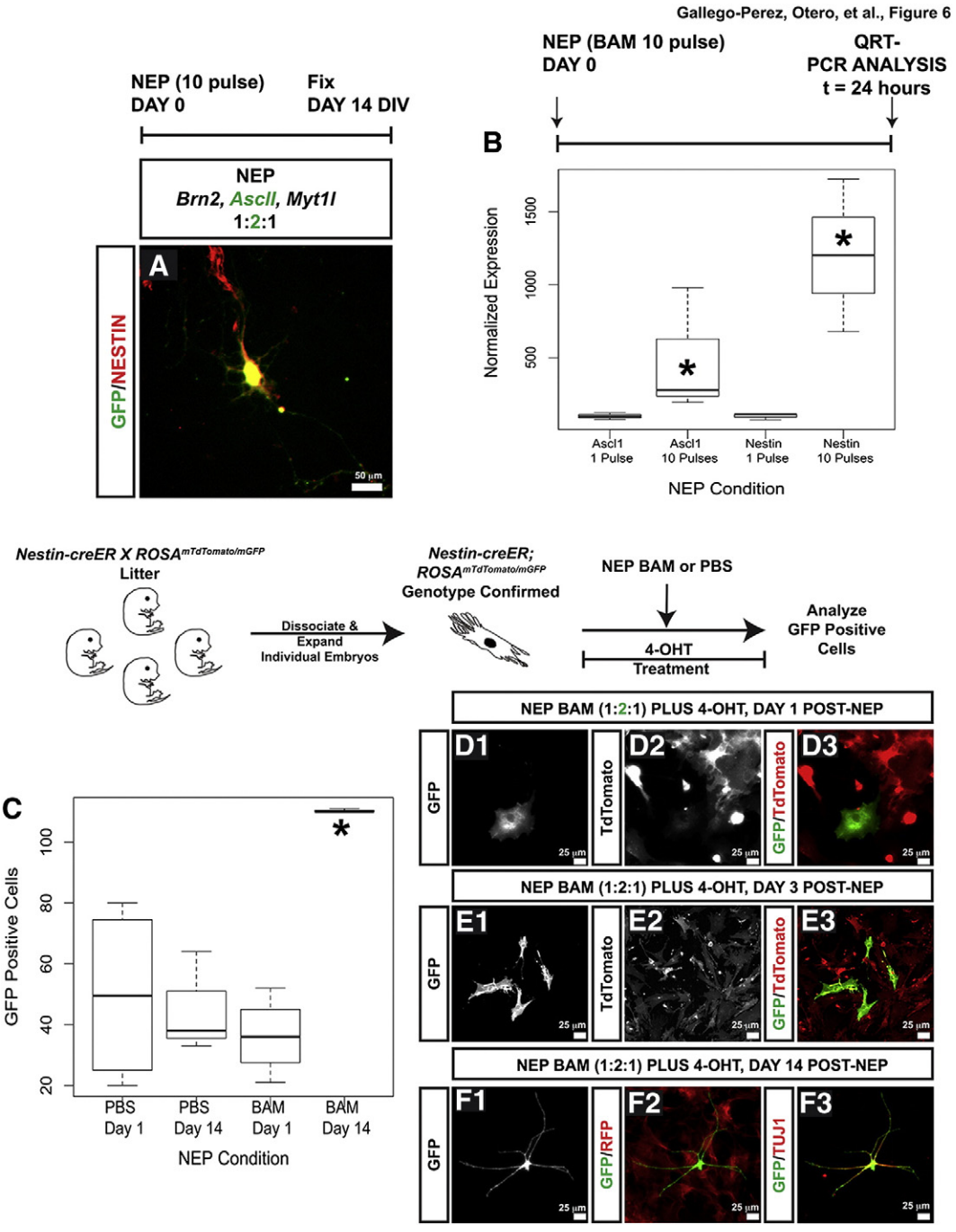

Figure 6. BAM-mediated induced neuron formation by NEP generates nestin-positive cells.**(A)** GFP and nestin co-expression indicates that a subset of *Ascl1-IRES-GFP* expressing cells show nestin immunoreactivity.**(B)** *Ascl1* and *Nestin* qRT-PCR demonstrate increased exogenous *Ascl1* expression after 10 NEP pulses of BAM and increased endogenous nestin expression after 10 NEP pulses of BAM (asterisk indicates $P < 0.05$). Schematic shows general methodology to test for nestin induction during BAM-mediated neuronal reprogramming.**(C)** Quantification of GFP positive cells after NEP of either phosphate buffered saline (PBS) or BAM. Note that by day 14, a significant population of GFP-positive cells is noted indicating increased cre-mediated recombination.**(D-F)** Epifluorescent photomicrographs at different stages of the reprogramming of MEFs derived from *Nestin-cre-ER, Rosa*$^{mTdTomato/mGFP}$ mice treated with BAM (1:2:1 ratio) plus 4-OHT. Under these conditions, cre recombinase would be active in cells that express nestin. Panels D1-D3 are 1 day post plating. Panels E1-E3 are 3 days post-plating. Panels F1-F3 are 14 days post-plating. Molecular markers are delineated on the boxes to the left of the panel.

many GFP-positive neurons, indicating that the cells had passed through a *nestin*-positive stage (Figure 6, *F*). We conclude that at least a subset of fibroblasts transition through a *nestin*-positive state during BAM-mediated neuronal reprogramming. The implications of *nestin* gene expression during reprogramming raises the possibility that during iN generation, cells may pass through a neural progenitor phase. If this were to be the case, such transitions to a progenitor state would represent an

additional stochastic barrier to iN generation as *nestin*-positive progenitor cells generate both neurons and glia.

Discussion

NEP is an improved methodology for nuclear reprogramming applications

The current *status quo* for exogenous gene expression in nuclear reprogramming includes stochastic methodologies, such as viral infection and bulk electroporation (BEP) (reviewed by Bernal[21]). In this report we have moved against the *status quo* by adapting nanochannel electroporation (NEP) for nuclear reprogramming. NEP's advantages include (1) high transfection delivery with low toxicity, (2) more uniform gene delivery across a group of cells, (3) transfection scalability, and (4) the capacity to transfect many reprogramming/patterning genes simultaneously. Using this approach, we discovered a novel role for *CCNA2* in BAM-mediated neuronal reprogramming and have clarified the fate of MEFs during transition into neurons. Specifically, our data indicate that at least a subset of MEFs transition through a *nestin*-positive stage during BAM-mediated neuronal reprogramming.

Although the inclusion of multicistronic expression vectors or translated products capable of TEVP-mediated proteolysis theoretically can aid in controlling the ratios of reprogramming factors, they are fraught with caveats. First, the molar ratios achieved by implementing these methodologies will always be equimolar. Our data demonstrating that increased *AsclI* relative to *Brn2* and *MytlI* increases neuronal nuclear reprogramming efficiency and increases neuronal complexity underscore the importance of controlling relative levels of reprogramming genes during this process. Furthermore, NEP technology is not constrained to plasmid DNA delivery. Indeed, any charged molecule, including drugs, miRNA,[22] or RNA implicated in reprogramming,[23] can be delivered using NEP. Although viral based gene delivery methodologies such as Sendai virus may have unique advantages, viral gene delivery will always be constrained by capsid size; such constraints are not applicable to NEP. Plasmid size constraints hinder efficiency of gene editing tools such as dCas9, which are often over 9 kb in size.[24]

Stochastic barriers to efficient neuronal nuclear reprogramming

Somatic cell reprogramming into iPS cells has some technical advantages over neuronal reprogramming. Specifically, the fact that iPS cells have a significant proliferative potential indicates that they are amenable to clonal dilution and colony picking. In contrast, somatic cell reprogramming into neurons will ultimately require a high throughput methodology to generate neurons in sufficient quantities for regenerative medicine applications. With NEP technology, we are uniquely capable of delivering in a benign fashion a precise dosage of reprogramming factors. Our findings show that NEP is an improved electroporation strategy relative to BEP in that we are capable of producing more neurons, NEP induced neurons display more complexly arborized neurites relative to bulk electroporation, and the reprogramming occurs faster. Nevertheless, with NEP we found that not all of the cells reprogrammed into neurons, and that induced neuron formation occurred at different rates, despite receiving more uniform quantities of plasmid DNA compared to BEP. Our data show that exogenous *Ascl1* transcripts may be endogenously silenced more rapidly than other factors, and that some cells undergo neuronal reprogramming more rapidly than others. Furthermore, the apparent dependency of S-phase cyclins for reprogramming underscores a potential prominent role of the cell cycle regulatory genes. Thus, NEP BAM-mediated neuronal reprogramming has several stochastic barriers downstream of the plasmid delivery that must be overcome. Indeed, these data are in keeping with the stochastic nature of OSKM-mediated somatic cell reprogramming into iPS cells.[25]

Ascl1 has been recently identified as the pioneer factor for neuronal reprogramming.[18] We have shown, for the first time, that uniform expression of BAM reprogramming factors alone does not guarantee neuronal reprogramming from MEFs. Our finding showing selective depletion of exogenous *Ascl1* transcription in some cells is in keeping with the notion that robust *Ascl1* expression is required for neuronal reprogramming. Indeed, endogenous silencing of exogenous *Ascl1* transcription seems to play a role in maintaining the stochastic nature to BAM-mediated neuronal reprogramming. Unraveling the mechanisms of this endogenous barrier may allow the acceleration of *synchronous* and *deterministic* neuronal reprogramming as has been shown in iPS cell reprogramming paradigms.[26] Nevertheless, the cellular mechanisms by which *Ascl1* promotes neuronal reprogramming are not fully understood. In the chick developing neural tube, exogenous murine *Ascl1* expression accelerates neuronal differentiation with concomitant cell cycle exit.[27] In contrast, in the murine ventral telencephalon, several pro-proliferative genes are enhanced directly by *Ascl1*, including several G1/S and G2/M-transition proteins; these genes are activated prior to classical *Ascl1*-associated genes implicated in neuronal specification with cell cycle exit.[28] It is therefore not surprising that targeted ablation of the S-phase gene *CCNA2* early during neuronal reprogramming hampers iN formation. These data suggest that early during the process, at least some reprogramming cells may require DNA replication, which is a known modifier of epigenetic signatures.[29] Furthermore, our data suggest that at least a subset of reprogrammed neurons proceed through a nestin-positive cell stage. In summary, our NEP platform has generated a framework upon which future experiments can be efficiently designed to dissect the molecular underpinnings of nuclear reprogramming and neuronal cellular maturity. Our novel biological findings uncover stochastic cellular mechanisms that explain to some extent the inefficiencies of induced neuron formation.

Author contributions

- NEP design, manufacturing, and validation were performed by Daniel Gallego-Perez, Veysi Malkoc, Junyu Ma, Wei-Ching Liao, Xi Zhao, Xinmei Wang, Andrew Adler, Kam Leong and L. James Lee.
- Design, implementation, and interpretation of reprogramming experiments, live cell imaging, transgenic mouse

experiments, histology, photomicroscopy, and neuronal morphometric studies were performed by Daniel Gallego-Perez, José J. Otero, Catherine Czeisler, Patrick Gygli, Fay Patsy Catacutan, Cristina Ortiz, Hamza Gokozan, Veysi Malkoc, Subhadip Ghatak, and Aaron Cowgill.

- *In utero* surgery experiments were developed, implemented, and validated by Brian Wulff, Subhadip Ghatak, Surya Gnyawali, Daniel Gallego-Perez, Traci A. Wilgus, Savita Khanna, Cameron Rink, and Chandan K. Sen
- Electrophysiology was performed and interpreted by Thomas Sherwood and Candice Askwith.
- The manuscript was written by José Javier Otero, Daniel Gallego-Perez, L. James Lee, and Chandan K. Sen with significant feedback and proofreading from all authors.

Appendix A. Supplementary data

Supplementary data to this article can be found online at http://dx.doi.org/10.1016/j.nano.2015.11.015.

References

1. Takahashi K, Yamanaka S. Induction of pluripotent stem cells from mouse embryonic and adult fibroblast cultures by defined factors. *Cell* 2006;**126**:663-76.
2. Vierbuchen T, Ostermeier A, Pang ZP, Kokubu Y, Sudhof TC, Wernig M. Direct conversion of fibroblasts to functional neurons by defined factors. *Nature* 2010;**463**:1035-41.
3. Li Z, Rana TM. A kinase inhibitor screen identifies small-molecule enhancers of reprogramming and iPS cell generation. *Nat Commun* 2012;**3**:1085.
4. Li K, Zhu S, Russ HA, Xu S, Xu T, Zhang Y, et al. Small molecules facilitate the reprogramming of mouse fibroblasts into pancreatic lineages. *Cell Stem Cell* 2014;**14**:228-36.
5. Wang H, Cao N, Spencer CI, Nie B, Ma T, Xu T, et al. Small molecules enable cardiac reprogramming of mouse fibroblasts with a single factor, Oct4. *Cell Rep* 2014;**6**(5):951-60.
6. Liu ML, Zang T, Zou Y, Chang JC, Gibson JR, Huber KM, et al. Small molecules enable neurogenin 2 to efficiently convert human fibroblasts into cholinergic neurons. *Nat Commun* 2013;**4**:2183.
7. Ladewig J, Mertens J, Kesavan J, Doerr J, Poppe D, Glaue F, et al. Small molecules enable highly efficient neuronal conversion of human fibroblasts. *Nat Methods* 2012;**9**:575-8.
8. Geng T, Lu C. Microfluidic electroporation for cellular analysis and delivery. *Lab Chip* 2013;**13**:3803-21.
9. Boukany PE, Morss A, Liao WC, Henslee B, Jung H, Zhang X, et al. Nanochannel electroporation delivers precise amounts of biomolecules into living cells. *Nat Nanotechnol* 2011;**6**:747-54.
10. Sun C, Cao Z, Wu M, Lu C. Intracellular tracking of single native molecules with electroporation-delivered quantum dots. *Anal Chem* 2014;**86**:11403-9.
11. Ma S, Schroeder B, Sun C, Loufakis DN, Cao Z, Sriranganathan N, et al. Electroporation-based delivery of cell-penetrating peptide conjugates of peptide nucleic acids for antisense inhibition of intracellular bacteria. *Integr Biol (Camb)* 2014;**6**:973-8.
12. Okita K, Hong H, Takahashi K, Yamanaka S. Generation of mouse-induced pluripotent stem cells with plasmid vectors. *Nat Protoc* 2010;**5**:418-28.
13. Adler AF, Grigsby CL, Kulangara K, Wang H, Yasuda R, Leong KW. Nonviral direct conversion of primary mouse embryonic fibroblasts to neuronal cells. *Mol Ther Nucleic Acids* 2012;**1**:e32.
14. Chen X, Pham E, Truong K. TEV protease-facilitated stoichiometric delivery of multiple genes using a single expression vector. *Protein Sci* 2010;**19**:2379-88.
15. Hirai H, Tani T, Katoku-Kikyo N, Kellner S, Karian P, Firpo M, et al. Radical acceleration of nuclear reprogramming by chromatin remodeling with the transactivation domain of MyoD. *Stem Cells* 2011;**29**:1349-61.
16. Levanon D, Brenner O, Negreanu V, Bettoun D, Woolf E, Eilam R, et al. Spatial and temporal expression pattern of Runx3 (Aml2) and Runx1 (Aml1) indicates non-redundant functions during mouse embryogenesis. *Mech Dev* 2001;**109**:413-7.
17. Brunet JF, Pattyn A. Phox2 genes—from patterning to connectivity. *Curr Opin Genet Dev* 2002;**12**:435-40.
18. Wapinski OL, Vierbuchen T, Qu K, Lee QY, Chanda S, Fuentes DR, et al. Hierarchical mechanisms for direct reprogramming of fibroblasts to neurons. *Cell* 2013;**155**:621-35.
19. Katsuno Y, Suzuki A, Sugimura K, Okumura K, Zineldeen DH, Shimada M, et al. Cyclin A-Cdk1 regulates the origin firing program in mammalian cells. *Proc Natl Acad Sci U S A* 2009;**106**:3184-9.
20. Kim J, Su SC, Wang H, Cheng AW, Cassady JP, Lodato MA, et al. Functional integration of dopaminergic neurons directly converted from mouse fibroblasts. *Cell Stem Cell* 2011;**9**:413-9.
21. Bernal JA. RNA-based tools for nuclear reprogramming and lineage-conversion: towards clinical applications. *J Cardiovasc Transl Res* 2013;**6**:956-68.
22. Guo X, Liu Q, Wang G, Zhu S, Gao L, Hong W, et al. microRNA-29b is a novel mediator of Sox2 function in the regulation of somatic cell reprogramming. *Cell Res* 2013;**23**:142-56.
23. Warren L, Manos PD, Ahfeldt T, Loh YH, Li H, Lau F, et al. Highly efficient reprogramming to pluripotency and directed differentiation of human cells with synthetic modified mRNA. *Cell Stem Cell* 2010;**7**:618-30.
24. Perez-Pinera P, Kocak DD, Vockley CM, Adler AF, Kabadi AM, Polstein LR, et al. RNA-guided gene activation by CRISPR-Cas9-based transcription factors. *Nat Methods* 2013;**10**:973-6.
25. Hanna J, Saha K, Pando B, van Zon J, Lengner CJ, Creyghton MP, et al. Direct cell reprogramming is a stochastic process amenable to acceleration. *Nature* 2009;**462**:595-601.
26. Rais Y, Zviran A, Geula S, Gafni O, Chomsky E, Viukov S, et al. Deterministic direct reprogramming of somatic cells to pluripotency. *Nature* 2013;**502**:65-70.
27. Nakada Y, Hunsaker TL, Henke RM, Johnson JE. Distinct domains within Mash1 and Math1 are required for function in neuronal differentiation versus neuronal cell-type specification. *Development* 2004;**131**:1319-30.
28. Castro DS, Martynoga B, Parras C, Ramesh V, Pacary E, Johnston C, et al. A novel function of the proneural factor Ascl1 in progenitor proliferation identified by genome-wide characterization of its targets. *Genes Dev* 2011;**25**:930-45.
29. Li B, Su T, Ferrari R, Li JY, Kurdistani SK. A unique epigenetic signature is associated with active DNA replication loci in human embryonic stem cells. *Epigenetics* 2014;**9**:257-67.